THE JOURNAL OF PHYSICAL CHEMISTRY C

Article

Stability and Electronic Properties of Atomistically-Engineered 2D Boron Sheets

Kah Chun Lau, and Ravindra Pandey

J. Phys. Chem. C, **2007**, 111 (7), 2906-2912 • DOI: 10.1021/jp066719w

Stability and Electronic Properties of Atomistically-Engineered 2D Boron Sheets

Kah Chun Lau and Ravindra Pandey*

Department of Physics, Michigan Technological University, Houghton, Michigan 49931

Received: October 12, 2006; In Final Form: November 28, 2006

First principles calculations based on generalized-gradient approximation to density functional theory are performed to study structural and electronic properties of the 2D sheets consisting of the elemental boron. The results find that the boron sheet can be stable and can possess metallic or semiconducting character depending on its atomistic configuration. The unique features present in the electronic properties of the buckled {1212} and reconstructed {1221} sheets would lead to a significant variation on electronic and mechanical properties of the corresponding single-walled boron nanotubes.

I. Introduction

Elemental structures, in general, have always played a pivotal role in the physics and chemistry of materials; they not only give insight into the properties of the elements but also pose challenging questions in their own right. The elemental boron holds a unique place among the elements of the periodic table by having the most varied polymorphism, which includes novel nanostructures (e.g., nanowires,[1] nanoribbons,[2] nanotubes[3] and nanoclusters[4−8]), and complex icosahedral networks observed in the conventional boron-rich solids.[9−13] Similar to carbon-based nanostructures (e.g., fullerenes[14] and nanotubes[15]), which are formed only under kinetically constrained conditions, boron-based nanostructures have also been envisioned,[16−22,23−25] though their properties have not yet been fully elucidated. A recent study of the syntheses of elemental single-walled boron nanotubes (SWBNTs),[3] together with prediction of ballistic conduction in SWBNTs[26] have certainly raised the expectation of their role in the next-generation devices for novel technological applications.

One of the main difficulties in synthesizing boron nanotubes appears to be the instability of a graphene-like boron sheet. It is mainly due to the fact that, in contrast to carbon, multicentered bonds and electron-deficient features of boron[9,27] are energetically more competitive and stable than bonding features with only the sp^2 hybridization. In spite of this fact, single-walled boron nanotubes were proposed by folding a hypothetical triangular boron sheet that was constructed by the hexagonal pyramidal B_7 units.[18] It is to be noted here that stability and electronic properties of such a triangular boron sheet have so far not been verified by experiments.

Our group has recently performed a theoretical study to investigate energetics and electronic properties of a boron sheet and the corresponding boron nanotubes.[22] The preliminary results based on density functional theory (DFT) within the generalized gradient approximation (GGA) show the relative stability of the sheet reconstructed from the planar triangular lattice.[22] On the other hand, the calculations based on local density approximation (LDA) in density functional theory find the ground state of a boron sheet to consist of a buckled triangular lattice.[21,23,24] Because neither GGA-DFT nor LDA-DFT calculations have resulted in an exhaustive search for the geometric configurations that can be considered for the stable configurations, the nature of the ground state of a 2D boron sheet still remains an open question, which we address in the present study.

We have organized the rest of the paper as follows. The computational method used in this work is presented in section II. In section III, we present and discuss our results, and we give a summary of the work in section IV.

II. Methodology

Electronic structure calculations were performed under the framework of density functional theory with the Perdew−Wang (PW91) exchange and correlation functionals.[28] A plane wave basis set was used, and the valence-core interaction was described by the ultrasoft pseudopotential (US-PP)[29] as implemented in the Vienna ab initio simulation package (VASP).[30] In the course of both the cell parameters and atomic positions optimization, the *k*-space integrations were carried out using the method of Methfessel and Paxton[31] in the first order, with employed smearing width of 0.05 eV. An energy cutoff of 260 eV in the plane wave expansion and of 443 eV for the augmented charge was used. The sizes of the *k*-point sampling for different systems with different unique cells were individually converged, with a precision of 5 meV/atom. For each optimized structure, total energy was again calculated by using the tetrahedron method with Blöchl corrections using the cutoff energy value of 320 eV in the plane wave expansion as used in VASP.

The reliability and accuracy of the computational model employed was tested on the well studied boron crystalline solid, α-B_{12}, which occurs in the rhombohedral phase at ambient pressure and temperature. Table 1 shows that the model parameters used in the current study have successfully reproduced the results of previous theoretical[10,11,21,23] and experimental[32,33] studies on α-B_{12} solid. Both LDA (i.e., using the Perdew−Zunger−Ceperley−Alder exchange-correlation functional) and GGA results predict very similar values of the structural parameters, though the LDA overestimates the binding energies.

We have used the same set of model parameters for calculations of the boron sheet that were used for elemental structure calculations of α-B_{12}. For the monolayer boron sheet, a supercell was constructed by placing a basic unit of the sheet

* Corresponding author. E-mail: pandey@mtu.edu.

10.1021/jp066719w CCC: $37.00
Published on Web 01/26/2007

TABLE 1: Binding Energy (BE, eV/atom) and Geometrical Parameters[a] for α-B_{12} Boron Solid

model	ref	BE	d_{intra}	d_{inter}	a
LDA	this work	7.10	1.72, 1.76, 1.77	1.65, 1.97	4.97
	23	6.84			
	21	7.37			
GGA	this work	6.18	1.74, 1.77, 1.80	1.66, 2.00	5.04
	23	6.22			
	10	6.95		1.67, 1.99	4.98
	11		1.72, 1.76, 1.78	1.65, 1.98	4.98
experiment	32, 33	5.81		1.71, 2.02	5.06

[a] d_{intra} is the intra-icosahedral bond length, d_{inter} is the inter-icosahedral, and a is the lattice parameter. The unit is Å.

in the *xy*-plane inside a rectangular grid with a surface-to-surface separation of ~10 Å in the *z*-direction, which ensures a negligible interaction between the sheet and its image. In general, the configurations considered for the sheet were built by repeating the basic unit which is composed of 8−12 boron atoms depending on a given configuration. The Brillouin zone was sampled using a 8 × 8 × 8 Monkhorst−Pack grid for the integration in the reciprocal space. Calculations were deemed converged when changes in total energy were less than 10^{-5} eV and those in the interatomic forces were less than 0.01 eV/Å. Additional details of the calculations can be found elsewhere.[34]

III. Results and Discussion

Owing to its vast variety of structures and complexity in bonding features, a full understanding of properties of boron nanostructures is not likely to be an easy task. Boron has three valence electrons and a short covalent radius. It can undergo sp^2 hybridization in forming atomic clusters that leaves one unoccupied $2p_z$ atomic orbital rendering boron to be electron-deficient.[9] Consequently, the 2D planar and quasi-planar boron clusters are found to be benefitted from π-delocalization due to the unoccupied $2p_z$ orbitals. In fact, the anomalous stability of these planar boron clusters is attributed to aromaticity arising from π-electrons.[7,35−39]

Due to its electron-deficient character, multicentered bonds are expected to help in understanding the way boron atoms tend to interact with each other. For example, dominance of three-centered bonds in boron compounds precludes the formation of chains or rings in boron clusters[5,40] and leads to the importance of a B−B−B unit in boron chemistry. In this case, a three-center bond generally involves two electrons in a localized molecular orbital formed by three atomic orbitals (AOs) directed toward the center of the triangle.[9,27] Realizing that the boron atoms tend to assume the geometries that are based on polyhedra or fragments of a polyhedra in which triangular faces prevail, our choice of sheet configurations for DFT calculations will be based on the interplay of the bonding features, overlap of the atomic orbitals, and geometrical features in the formation of the 2D boron sheet with respect to the 3D boron crystal.

Becasue the previous studies[21,23,24,22] on the boron sheet were limited in sampling the potential energy landscape, calculations were performed by considering a diverse and extensive set of initial configurations with and without symmetry constraints. The resulting optimized configurations are then classified into different categories to provide a better representation of the potential energy landscape of the boron sheet.

A. Structural Properties. Figure 1 displays the several sheet configurations divided into several distinct categories, namely hexagonal graphene-like sheet, idealized and buckled {1212} sheets, reconstructed {1221} sheets, sheets based on the icosahedral configuration, low-symmetry sheets, and hybrid sheets. It is to be noted that our preliminary work considered only idealized {1212} and reconstructed {1221} sheet configurations.[22]

Expecting the resemblance of the polymorphism of boron crystalline solids with that of boron sheets, some of the structural features can be extracted from the configurational parameters given in Table 2. Most of the sheet geometries have ~90−92% of the binding energy of the α-B_{12} solid, and the atomic arrangements can be found to have variations of those in the triangular {1212} lattice. The flat {1212} sheet has a 6-fold coordination of boron atoms, which is uniformly repeated in a basic triangular three-atom unit. In fact, this terminology can be derived through a planar projection of Aufbau principle[4] where the motifs consisting of a pentagonal pyramidal B_6 and the hexagonal pyramidal B_7 are found to be the basic unit to form elemental boron clusters. The calculated cohesive energy of the flat {1212} sheet is 5.48 eV/atom, higher than that of the sp^2-bonded hexagonal graphene-like boron sheet, which is only 4.96 eV/atom (Table 2). When the symmetry of the flat sheet is broken, we find several degenerate metastable buckling configurations depending on the degree and direction of buckling. The structural details of these configurations can be obtained from one of the authors (kclau@mtu.edu).

The calculated results find the buckled {1212} sheet to be the most stable configuration with cohesive energy 5.70 eV/atom, achieving ~92% of stability of the α-B_{12} solid. The buckling has induced stability with $\Delta E = 0.22$ eV/atom over the flat {1212} sheet. The order of the stabilization energy introduced by the buckling is in agreement with the previous theoretical studies,[21,23,24] as shown in Table 3. The optimized puckering height of 0.93 Å, is also comparable with the reported LDA height of 0.82−0.85 Å.[23,24]

Among all the planar isomers, the reconstructed {1221} boron sheet turns out to be the most stable configuration. It is ~0.10 eV/atom more stable than its next competitive planar isomer, the idealized {1212} sheet. Instead of favoring the pure sp^2 graphene-like structure, the reconstructed configuration settles down to a "distorted" hexagonal unit yielding a triangular-square-triangular unit network. Such a network facilitates the charge transfer, thereby forming a strong localized σ-bond with a bond length 1.63 Å. In contrast to the case of the flat {1212} sheet, buckling of reconstructed {1221} boron sheet does not appear to enhance its stability (Table 2).

We also find several stable configurations, other than those in the {1212} category. Despite the predicted instability of the isolated B_{12} icosahedral configuration[41] in the small boron cluster regime, the 2D sheet consisting of the icosahedral network of boron atoms (i.e., icosahedral-I in Table 2) is the second lowest isomer with the binding energy of ~5.60 eV/atom. The icosahedral boron sheet mimics its bulk structure, and the average inter-icosahedral, (R_{inter}) and intra-icosahedral bond, (R_{intra}) are nearly the same as those in the α-B_{12} solid. Another competitive isomer arising due to a different cluster orientation (i.e., icosahedral-II) is separated by only 0.09 eV.

Knowing that the nearly flat energy surface requires the use of more accurate methods for total energy calculations, Table 3 shows the calculated results obtained using the projector augmented wave (PAW) method for three representative sheet configurations. Although the PAW method is computationally intensive, it is known to provide relatively more accurate energy than the ultrasoft pseudopotentials[29] (US-PP) within DFT.[42,43] To get a consistent comparison among different schemes (i.e.,

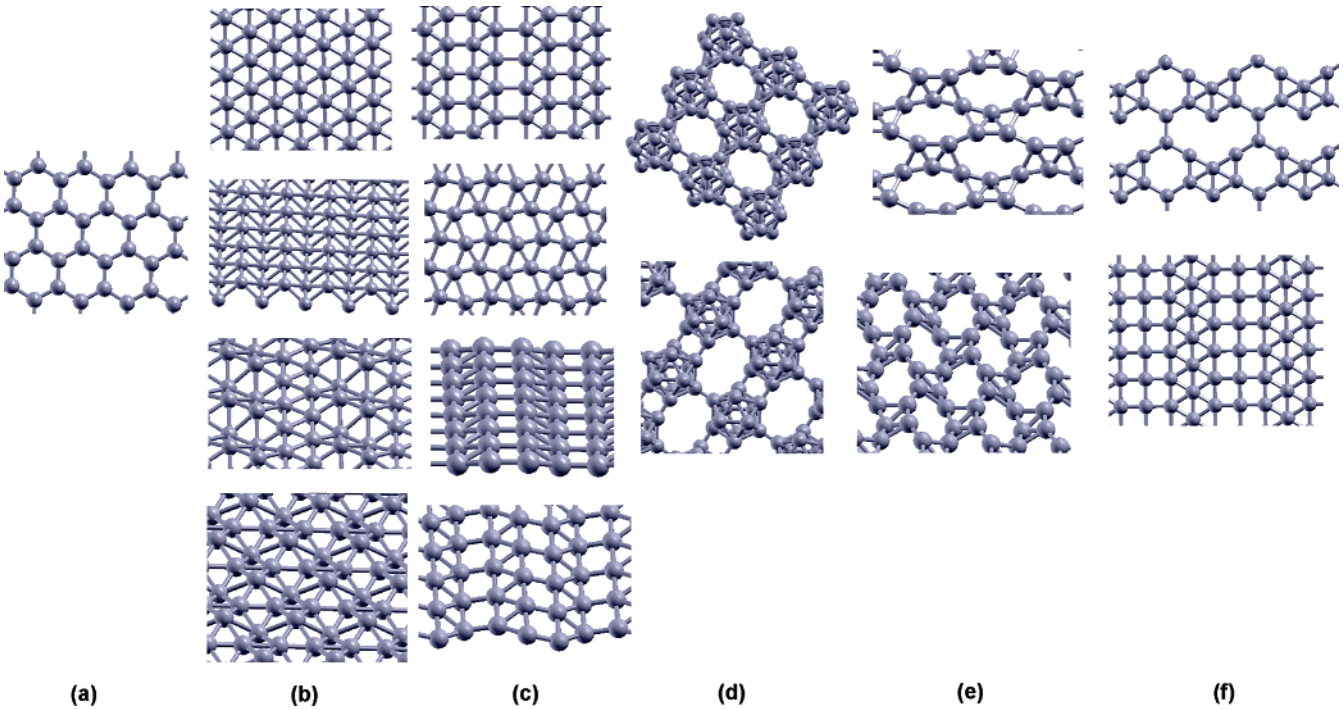

Figure 1. Boron sheets: (a) hexagonal graphene-like; (b) idealized and buckled {1212}; (c) reconstructed {1221}; (d) icosahedral; (e) low symmetry; (f) hybrid.

TABLE 2: Symmetry, Binding Energy (BE, eV/atom), Relative Stability with Respect to the Buckled {1212} (ΔE, eV/atom), and Bond Lengths (R_{B-B}, Å) Based on GGA Results for the Boron Sheet

sheet configuration	point symmetry	BE	ΔE	R_{B-B}
buckled {1212}	C_1	5.70	0.00	1.61, 1.89
icosahedral-I	C_{1h}	5.60	0.10	1.77[a] 1.63[b]
buckled "twisted-helix"	C_1	5.59	0.11	1.56, 1.61, 1.64 1.78
reconstructed {1221}	C_{1h}	5.57	0.13	1.63, 1.66, 2.00
buckled {1221}	C_1	5.57	0.13	1.69, 1.76
buckled {1212}-II	C_1	5.54	0.16	1.65, 1.78
icosahedral-II	C_{1h}	5.51	0.19	1.84[a] 1.75[b]
idealized {1212}	C_{2h}	5.48	0.22	1.71
hybrid	C_1	5.35	0.35	1.61, 1.68, 1.92
hexagonal graphene-like	C_{2v}	4.96	0.74	1.68

[a] $\langle R_{intra} \rangle$. [b] $\langle R_{inter} \rangle$.

US-PP and PAW), we have used the same set of model parameters for all calculations, as we mentioned in section II. The GGA-DFT calculations in terms of either US-PP or PAW predict the reconstructed {1221} sheet to be energetically preferable ($\Delta E \sim 0.10$ eV/atom) to the flat idealized {1212} sheet. At the LDA-DFT level, however, both methods (i.e., US-PP and PAW) find the reconstructed {1221} sheet to be nearly degenerate with the idealized {1212}.

We note that the reconstructed {1221} boron sheet can be visualized as an assembly of the ground state configuration of B_6 unit in D_{2h} symmetry[44,4] with aromaticity in bonding that facilitates extra stability over the other planar configurations, such as the idealized {1212} sheet.[44] To enhance the extra stability of the planar {1212} boron sheet, "buckling" has to be induced to facilitate stronger localized bonds in the network. Table 3 also collects the LDA and GGA results for the buckled {1212} sheet, which are consistent in both US-PP and PAW models and are in agreement with the previous LDA studies.[21,23,24]

B. Chemical Bonding. We will now begin analysis of the chemical bonding knowing that stability of a given sheet configuration is controlled by an interplay of the valence electrons with its atomistic configuration. Indeed, we find that the atomic coordination index, Z (i.e., number of nearest neighbors of a given atom in the 2D network) essentially determines the bonding features and stability of a given sheet. Furthermore, a combination of the localized two-center (2c) and delocalized three-center (3c) covalent bonds network which threads through atoms on the icosahedron surface to stabilize the lattice of a conventional 3D boron crystalline solid[9−13,45,27] plays a vital role in determining the stability of the boron sheet.

In α-B_{12}, boron atoms tend to form multicenter bonds in addition to two-center two-electron covalent bonds between neighboring icosahedra, which typically appear at high electron density region of ∼0.95 e/Å^3 (Figure 2-AI). There are intracluster 3c bonds on the twenty triangular planes of an icosahedron at low-density region of 0.77 e/Å^3 (Figure 2-AII), and a relatively weaker intercluster (3*c*) bond at a low-density region of ∼0.60 e/Å^3 (Figure 2-AIII) among three icosahedra on a (111) plane of rhombohedral lattice.[9−12] It therefore helps us in explaining why the isolated B_{12} icosahedral unit is not stable in the small cluster regime[5,41,37] without the coexistence of both intra- and inter-icosahedron bonds. Indeed, such subtle bonding characters are present in the 2D icosahedral-based (i.e., icosahedral-I and -II) boron sheets.

Being one of the energetically competitive isomers among the boron sheets (see Table 2), the icosahedral-I sheet is being stabilized by both inter- and intra-icosahedral 2c σ-bonds with comparable strength (Figure 2-BI). In addition, a stronger intra-icosahedral 3c bond (Figure 2-BII) appears, which can be interpreted as the preservation of the intrinsic stability of each individual icosahedron by the unusual 3c bonds, where the electron-deficient nature of bonding forces electrons to be shared

TABLE 3: Binding Energy (BE, eV/atom) and the Bond Lengths (R_{B-B}, Å) for the Buckled and Idealized {1212} and Reconstructed {1221} Sheet Configurations

		idealized {1212}		buckled {1212}		reconstructed {1221}	
ref	model	BE	R_{B-B}	BE	R_{B-B}	BE	R_{B-B}
this work	LDA	6.36	1.69	6.54	1.60, 1.83	6.33	1.62, 1.64, 1.92
	PAW-LDA	6.39	1.70	6.57	1.60, 1.83	6.37	1.62, 1.65, 1.97
this work	GGA	5.48	1.71	5.70	1.61, 1.89	5.57	1.63, 1.66, 2.00
	PAW-GGA	5.69	1.71	5.92	1.61, 1.88	5.78	1.63, 1.66, 2.01
21	LDA	6.53		6.79			
23	LDA	6.06	1.70	6.27	1.63, 1.81		
24	LDA	6.76	1.69	6.94	1.60, 1.82		
23	GGA	5.49	1.71	5.72	1.64, 1.82		

at the triangular surfaces of the icosahedron. However, in contrast to α-B_{12}, the icosahedral-I sheet has no inter-icosahedral 3c bonds (Figure 2-BIII) at a low electron density of 0.63 e/Å^3, as compared to the solid that possesses fairly strong inter-icosahedral 3c bonds at 0.60 e/Å^3 shown in Figure 2-AIII. Therefore, it might explain why the 2D icosahedral boron sheet cannot be the lowest energy isomer due to the absence of the inter-icosahedral 3c bond, which utilizes the 3D space configuration, despite the unsaturated dangling bonds on its surface.

In the {1212} category, the atomic coordination index, *Z*, essentially determines the bonding features and stability of a given boron sheet. In the flat idealized {1212} sheet, the presence of the degenerate *p*-orbitals makes the highly symmetrical planar {1212} sheet less energetically stable (Table 2). Here, the atomic environment with the high coordination number (i.e., $Z = 6$) and the electron-deficient character yield the nearly homogeneous delocalized bonds (Figure 3-AI). A homogeneous charge density distribution associated with de-

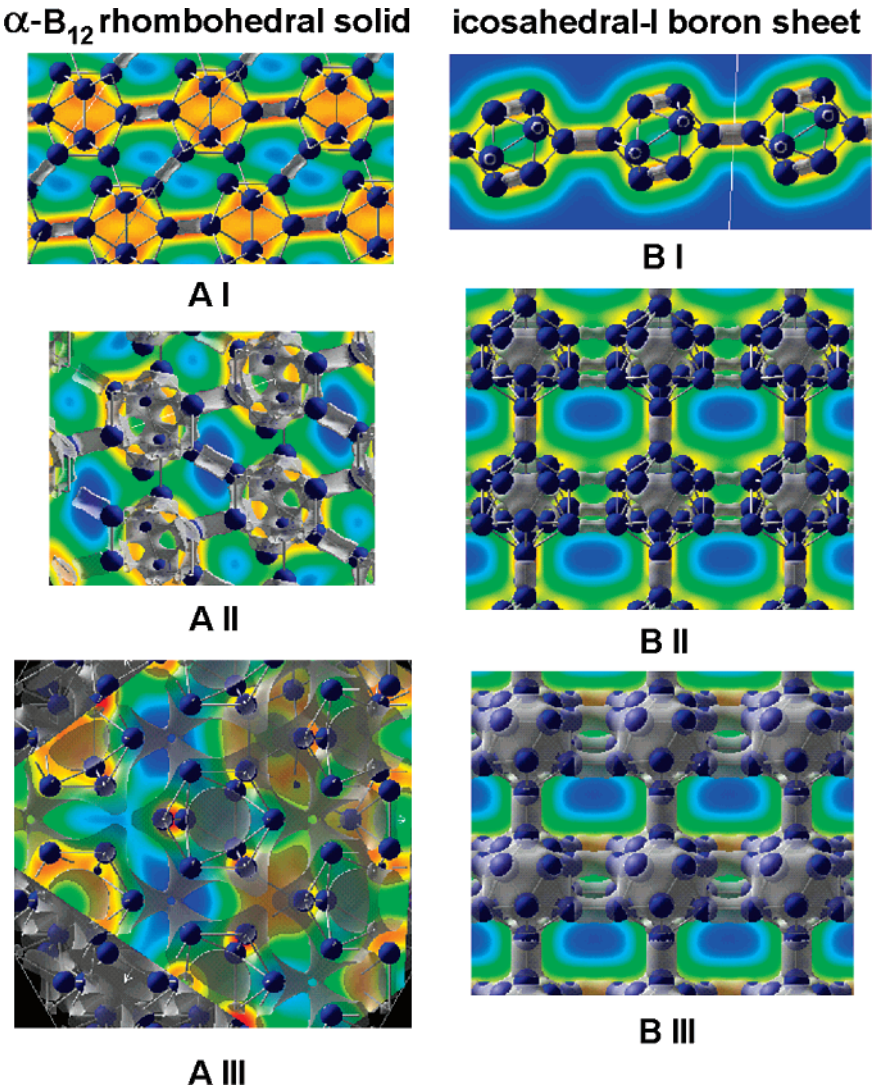

Figure 2. Equidensity surfaces of electron density with the section contour maps of the icosahedral based α-B_{12} solid (AI, AII, AIII) and the icosahedral-I boron sheet (BI, BII, BIII). The red region represents the high electron density contour, and the low electron density contour is shown by the blue region. The bonding is represented by the gray isosurfaces. The AI-2c inter-icosahedral bond is at 0.95 e/Å^3. The AII-3c intra-icosahedral bond is at 0.77 e/Å^3. The AIII-3c inter-icosahedral bond is at 0.60 e/Å^3. The BI-2c inter- and intra-icosahedral bonds are at 0.94 e/Å^3. The BII-3c intra-icosahedral bond is at 0.91 e/Å^3. The BIII-3c inter-icosahedral bond cannot be found at 0.63 e/Å^3.

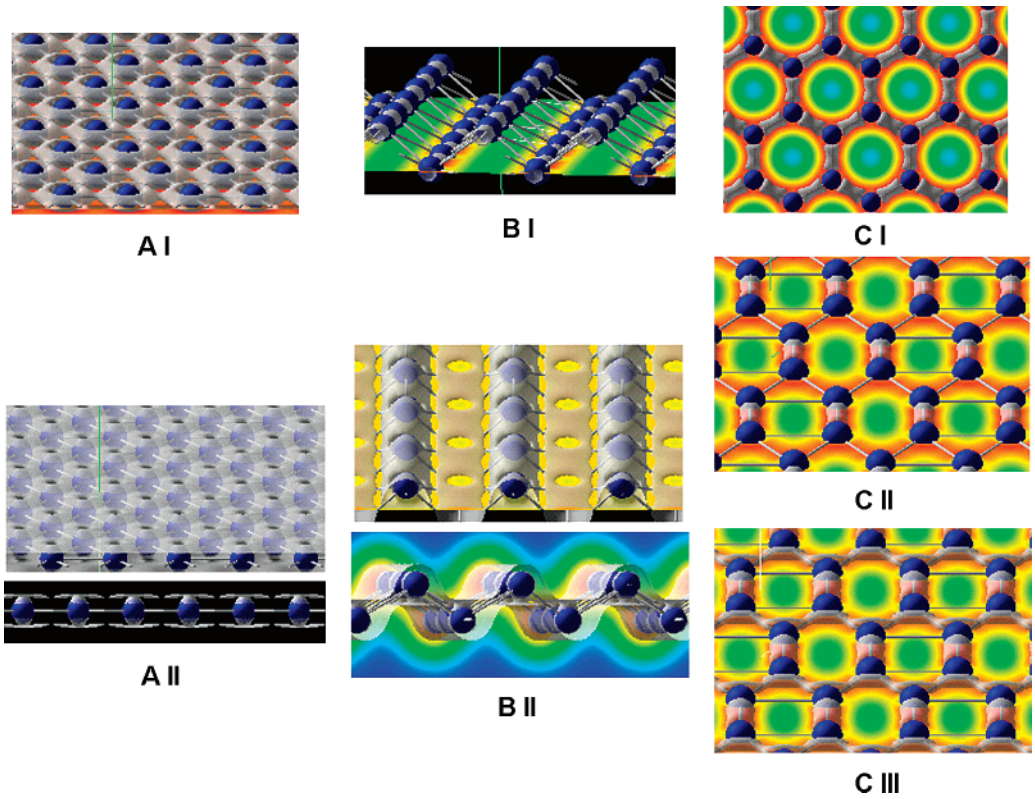

Figure 3. Equidensity surfaces of electron density with the section contour maps for the idealized {1212} (AI, AII), buckled {1212} (BI, BII), graphene-like (CI), and reconstructed {1221} (CII, CIII). The red region represents the high electron density contour, and the low electron density contour is shown by the blue region. The bonding is represented by the gray isosurfaces. The isosurfaces are at 0.82 e/Å^3 (AI), 0.65 e/Å^3 (AII), 0.95 e/Å^3 (BI), 0.61 e/Å^3 (BII), 0.87 e/Å^3 (CI), 0.98 e/Å^3 (CII), and 0.87 e/Å^3 (CIII).

localized π-electrons is dominant, as shown in Figure 3-AII, for the density region around 0.65 e/Å^3.

When the symmetry of the planar sheet is broken by inducing the buckling height of 0.90 Å, the buckled {1212} sheet becomes the lowest energy configuration by gaining extra stability of the 0.22 eV/atom with $Z = 2$ and $Z = 4$ for the first and second nearest neighbors. Here, the puckering stabilizes the triangular sheet by inducing a strong directional σ-bond along the infinite boron chains (Figure 3-BI), which breaks the degeneracy of p orbitals. Also, the infinite long boron chains along the "hill" and "valley" rows are each connected by a more delocalized weaker $\sigma-\pi$ bond between the adjacent rows (Figure 3-BII), despite the chain-like configurations not being stable on their own in the cluster regime.[6,40] Therefore, similarly to the icosahedral clusters based configurations, the buckled {1212} sheet prefers a mixture of localized and delocalized covalent bonds, which is analogous to dominant features of a mixed 2c and 3c covalent bonded network.

Regarding the most stable planar 2D boron sheet, the reconstructed {1221} sheet can be viewed as a "distorted" hexagonal ring as compared to the graphene sheet. If the symmetry is altered, the reconstructed {1221} sheet has the atomic coordination index $Z = 1$ and $Z = 2$ for its first and second nearest neighbors in the triangular-square-triangular network, in contrast to $Z = 3$ for the sp^2-dominant (Figure 3-CI) hexagonal graphene-like sheet. In a planar configuration, it has been pointed out by Evans et al.[21] that boron has one less electron than carbon, which makes the domination of the bonding in the graphene-like sheet by both sp^2 and π bonds energetically unfavorable. It is likely to be why one cannot find the analogous graphene sheet for boron in nature.

In the reconstructed {1221} sheet, there exists anisotropic chemical bonding[22] with significant contributions from the both in-plane localized directional covalent (i.e., σ-bond) and delocalized 3c bonds spreading along the triangular lattice networks. The electron density distribution, shown in Figure 3-CIII, reveals that the charge transfer between the delocalized 3c bonds at 0.87 e/Å^3 in the network can be accommodated by the formation of directional covalent bonds (i.e., σ-bond) that interconnect the triangular units (Figure 3-CII). Analogous to the case of the solids (i.e., α-B_{12}),[9−13] it therefore appears that the coexistence of three-center and two-center covalent bonds makes the reconstructed {1221} sheet more stable relative to the pure sp^2-bonded graphene-like boron sheet. Hence, we believe, the mixture of 2c and 3c bonds found in several lower energy 2D sheet configurations in the present study might give us an insight in understanding and designing the boron-based novel nanostructures.

C. Electronic Properties. The electronic properties of the sheet configurations considered depend on their unique atomic arrangements and bonding features. The icosahedral-I and buckled "twisted-helix" boron sheets are semiconductors, and the rest of the boron sheets are metallic.

The semiconducting icosahedral-I boron sheet yields different features in its band diagram as compared to the metallic {1212} and reconstructed {1221} boron sheet. It possesses a rather flat band dispersion (Figure 4) for both valence and conduction bands. The icosahedral-I boron sheet has an indirect band gap of ~0.50 eV at Γ (Figure 4). Knowing that the conventional 3D boron crystalline solid (i.e., α-B_{12}) and boron nanowires[1] are semiconducting, we can attribute the semiconducting nature of the icosahedral sheet to the similarity of the atomistic and bonding features in the icosahedral-based configurations. Accordingly, the rich features of the p states around the top of the valence band (Figure 5) can be attributed to the localized directional inter-icosahedral σ-bonds. Whereas in the close

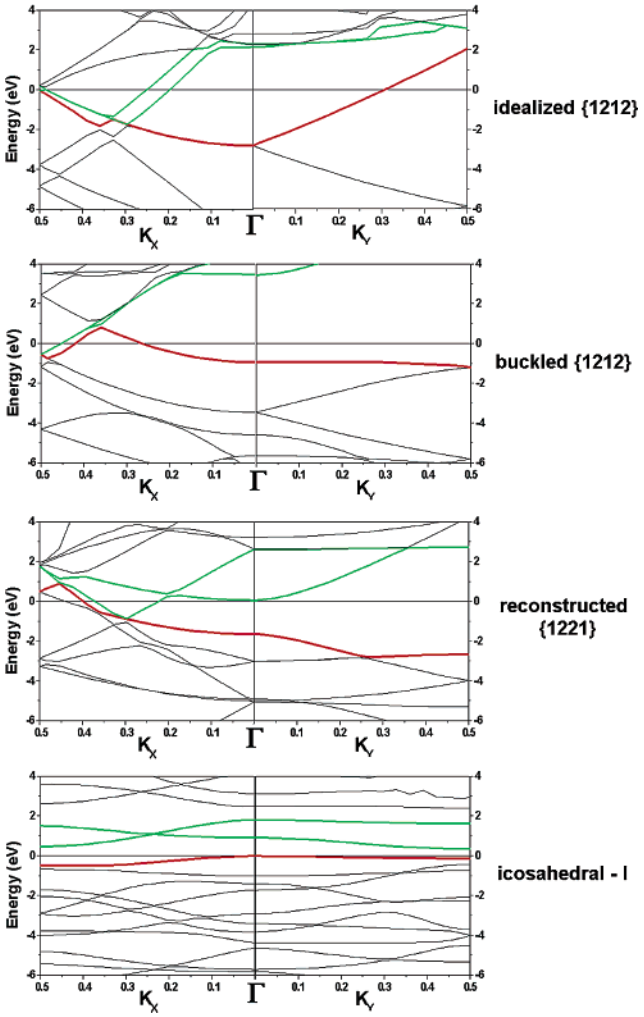

Figure 4. Band structure (from top to bottom) of the idealized {1212}, buckled {1212}, reconstructed {1221}, and icosahedral-I boron sheets. Zero is aligned to the Fermi energy. Red and green lines represent the valence and conduction bands, respectively.

proximity of bottom of the conduction bands, contributions of the overlap of s and p states can be seen in the projected density of states.

In contrast to the icosahedral-I boron sheet, dispersion of electronic bands is rather significant in the idealized {1212} sheet. The nearly homogeneous distribution of the electron cloud of the {1212} sheet leads to the isotropic metallic character in the band structure. A partially filled conduction band and strong overlap among valence and conduction bands can be seen in Figure 4, which also displays the isotropic features of metallic character in the band dispersion along the K_X and K_Y directions. The total density of states shown in Figure 5 indicates the appearance of the nonvanishing states near the vicinity of Fermi level, suggesting that the high electron conductivity is accessible in the {1212} sheet. From the calculated *l*-projected DOS, it can be seen that s and p states contribute equally to the conduction bands, and thereby indicate the occurrence of the s and p hybridization. Because the conduction bands are unoccupied, the no s states occupied feature found in the idealized {1212} sheet might be the cause of why it is energetically less favorable as compared to the others. Buckling of the {1212} sheet induces anisotropy in the band dispersion along K_X and K_Y directions (Figure 4). In the K_X direction, the conduction bands are partially filled ,suggesting a metallic-like character for the buckled {1212} sheet. The *l*-projected DOS identifies

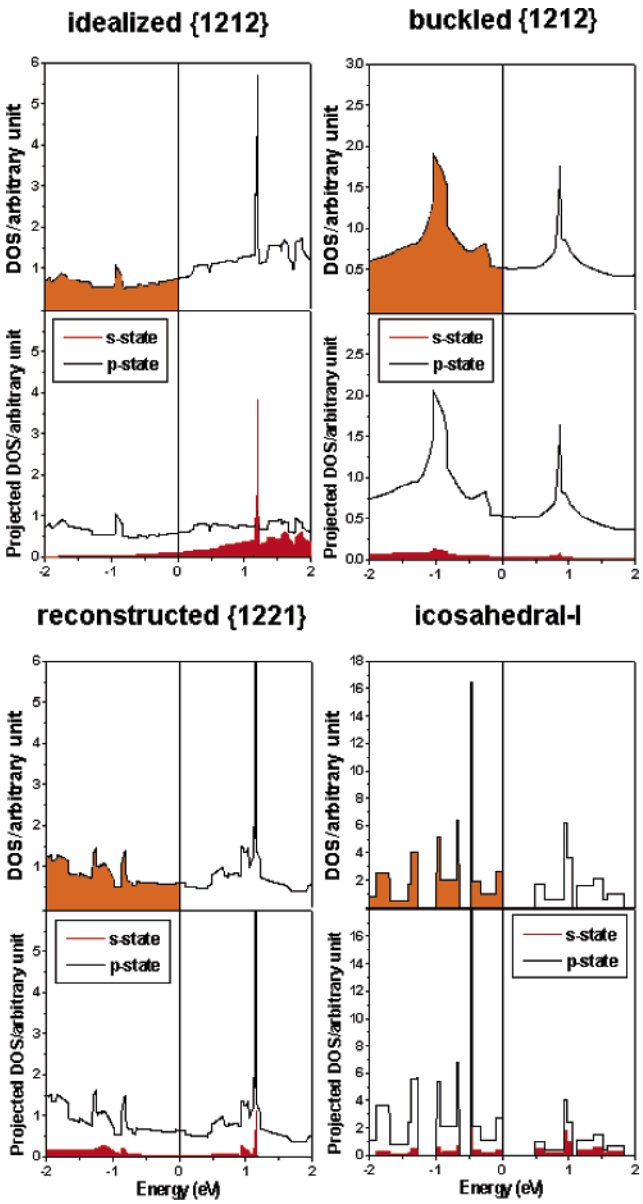

Figure 5. Total density of states, DOS (top panel), and *l*-projected s and p orbital in separated cases (bottom panel): (top left) idealized {1212} sheet; (top right) buckled {1212} sheet; (bottom left) reconstructed {1221} sheet; (bottom right) icosahedral-I boron sheet. Zero is aligned to the Fermi energy. The orange region in the top panel represents the occupied states in DOS, and the red region in the bottom panel represents the s orbital in *l*-projected DOS.

the top of the valence band and bottom of the conduction bands to be associated with π and π^* states, respectively.

In the reconstructed {1221} sheet, the anisotropic nature of the chemical bonding yields different dispersions along the K_X and K_Y directions (Figure 4) in its band structure. In contrast to the planar {1212} sheet, the *l*-projected DOS shows dominant features associated with the p state (i.e., p_y and p_z characteristics) in the proximity of the Fermi level (Figure 5). Accordingly, the rich features of the p states around the top of the flat valence band are attributed to the localized directional σ-bonds along the *Y* direction. They open up the gap (~0.8 eV) at Γ along the K_Y direction by lifting the degeneracy of the bands. On the other hand, the low-lying conduction bands are associated with the delocalized p_z-type π-bonding with bands crossing at Fermi level in the K_X direction. Similar to the case for the buckled {1212} sheet, anisotropic features of the chemical bonding together with its band dispersion in the reconstructed {1221} sheet suggest a

strong variation in the electronic and mechanical properties of the corresponding nanotubes, when the sheets are rolled into different chirality of single-walled boron nanotubes.

IV. Conclusions

In summary, first principles calculations were performed to study the stability, morphology and electronic properties of several sheet configurations of boron. Similar to those for the 3D boron solids, calculations predict a varied polymorphism in the 2D boron sheets, categorized into hexagonal graphene-like, idealized and buckled {1212}, icosahedral-like, reconstructed {1221}, low symmetry amorphous-like, and the hybrid 2D sheets. Among the planar sheet configurations, GGA-DFT calculations predict the stability of a novel reconstructed {1221} boron sheet over the idealized {1212} triangular sheet. Instead of having nearly homogeneous electron density on the 2D plane as in the case of the planar {1212} sheet, the reconstructed {1221} sheet is stabilized by coexistence of the localized σ-bonds and the delocalized three-center bonds.

The unique features in geometry and electronic properties of both {1212} and {1221} configurations suggest that a strong variation of electronic and mechanical properties is expected to occur when the plane is rolled into different chirality of single-walled boron nanotubes. Furthermore, the emergence of an icosahedral-based boron sheet as one of the low-lying configurations suggests the stability of inter-icosahedral and intra-icosahedral bonds, despite the fact that the discrete units of B_{12} icosahedral unit are not stable on their own in the small cluster regime. The most stable buckled {1212} sheet is found to be stabilized by the anisotropic bond properties due to the interplay between the localized σ-bonds and the delocalized superimpose $\sigma-\pi$-like bonds between the boron atoms in adjacent rows of boron chains.

Acknowledgment. This work was partially supported by DARPA through ARL Contract No. DAAD17-03-C-0115. We thank Dr. Roberto Orlando, S. Gowtham, Haiying He, and Dr. Mrinalini Deshpande for helpful comments and discussion during this work. We gratefully acknowledge CEC, MTU, for providing computational facility.

References and Notes

(1) Otten, J. C.; Lourie, O. R.; Yu, M.; Cowley, J. M.; Dyer, M. J.; Ruoff, R. S.; Buhro, W. E. *J. Am. Chem. Soc.* **2001**, *24*, 4564.
(2) Xu, T. T.; Zheng, J.; Wu, N.; Nicholls, W. A.; Roth, R. J.; Dikin, A. D.; Ruoff, R. S. *Nano Lett.* **2004**, *4*, 963.
(3) Ciuparu, D.; Klie, F. R.; Zhu, Y.; Pfefferle, L. *J. Phys. Chem. B* **2004**, *108*, 3967.
(4) Boustani, I. *Phys. Rev. B* **1997**, *55*, 16426.
(5) Lau, K. C.; Pandey, R. *Comput. Lett.* **2005**, *1*, 259 (Special Issue: Clusters).
(6) Lau, K. C.; Deshpande, D. M.; Pati, R.; Pandey, R. *Int. J. Quantum Chem.* **2005**, *103*, 866.
(7) Zhai, H.; Kiran, B.; Li, J.; Wang, L. S. *Nature Mater.* **2003**, *2*, 827.
(8) Kiran, B.; Bulusu, S.; Zhai, H.; Yoo, S.; Zheng, X.; Wang, L. S. *Proc Natl. Acad. Sci. U.S.A.* **2005**, *102*, 961.
(9) Muetterties, E. L., Ed. *The Chemistry of Boron and Its Compounds*; John Wiley: New York, 1967.
(10) Zhao, J.; Lu. J. P. *Phys. Rev. B* **2002**, *66*, 092101.
(11) Vast, N.; Baroni, S.; Zerah, G.; Besson, M. J.; Polian, A.; Grimsditch, M.; Chervin, J. C. *Phys. Rev Lett.* **1997**, *78*, 693.
(12) Fujimori, M.; Nakata, T.; Nakayama, T.; Nishibori, E.; Kimura, K.; Takata, M.; Sakata, M. *Phys. Rev. Lett.* **1999**, *82*, 4452.
(13) Shirai, K. *Phys. Rev. B* **1997**, *55*, 12235.
(14) Kroto, W. H.; Heath, R. J.; O'Brien, C. S.; Curl, F. R.; Smalley, R. E. *Nature (London)* **1985**, *318*, 162.
(15) Iijima, S. *Nature* **1991**, *354*, 56.
(16) Boustani, I.; Quandt, A *Europhys. Lett.* **1997**, *39*, 527.
(17) Gindulytu, A.; Lipscomb, N. W.; Massa, L. *Inorg. Chem.* **1998**, *37*, 6544.
(18) Boustani, I.; Quandt, A.; Hernández, E. Rubio, A. *J. Chem. Phys.* **1999**, *110*, 3176.
(19) Boustani, I.; Rubio, A.; Alonso, J. A. *Chem. Phys. Lett.* **1999**, *311*, 21.
(20) Kunstmann, J.; Quandt, A. *Chem. Phys. Lett.* **2005**, *402*, 21.
(21) Evans, H. M.; Joannopoulos, D. J.; Pantelides, S. T. *Phys. Rev. B* **2005**, *72*, 045434.
(22) Lau, K. C.; Pati. R.; Pandey, R.; Pineda, A. *C. Chem. Phys. Lett.* **2006**, *418*, 549.
(23) Cabria, I.; López, J. M.; Alonso, J. A. *Nanotechnology* **2006**, *17*, 778.
(24) Kunstmann, J.; Quandt, A. *Phys. Rev. B* **2006**, *74*, 035413.
(25) Zhang, D.; Zhu, R.; Liu, C. *J. Mater. Chem.* **2006**, *16*, 2429.
(26) Lau, K. C.; Pandey, R.; Pati, R.; Karna, S. P. *Appl. Phys. Lett.* **2006**, *88*, 212111.
(27) Muetterties, E. L., Ed. *Boron Hydride Chemistry*; Academic Press: New York, 1975.
(28) Perdew, P. J.; Wang, Y. *Phys. Rev. B* **1992**, *45*, 13244.
(29) Vanderbilt, D. *Phys. Rev. B* **1990**, *41*, 7892.
(30) Kresse, G.; Hafner, J.; VASP (Vienna, ab initio simulation package) software. Kresse, G.; Hafner, J. *Phys. Rev. B* **1993**, *47*, 558. Kresse, G; Furthmuller, J. *Phys. Rev. B* **1996**, *54*, 11169.
(31) Methfessel, M.; Paxton, A. T. *Phys. Rev. B* **1989**, *40*, 3616.
(32) Kittel, C. *Introduction to Solid State Physics*, 7th ed.; Wiley: New York, 1996.
(33) Donohue, J. *The Structure of The Elements*; Wiley: New York, 1974.
(34) Lau, K. C. Pandey, R. Unpublished work.
(35) Boustani, I. *Int. J. Quantum Chem.* **1994**, *52*, 1081.
(36) Fowler, E. J.; Ugalde, J. M. *J. Phys. Chem. A* **2000**, *104*, 397.
(37) Lau, K. C.; Deshpande, M.; Pandey, R. *Int. J. Quantum Chem.* **2005**, *102*, 656.
(38) Aihara, J. *J. Phys. Chem. A* **2001**, *105*, 5486.
(39) Aihara, J.; Kanno, H.; Ishida, T. *J. Am. Chem. Soc.* **2005**, *127*, 13324.
(40) Chacko, S.; Kanhere, G. D.; Boustani, I. *Phys. Rev. B* **2003**, *68*, 035414.
(41) Kawai, R.; Weare, J. H. *J. Chem. Phys.* **1991**, *95*, 1151.
(42) Blöchl, P. E. *Phys. Rev. B* **1994**, *50*, 17953.
(43) Kresse, G.; Joubert, D. *Phys. Rev. B* **1999**, *59*, 1758.
(44) Alexandrova, N. A.; Boldyrev, I. A.; Zhai, H.; Wang, L.; Steiner, E.; Fowler, P. W. *J. Phys. Chem. A* **2003**, *107*, 1359.
(45) Jemmis, D. E.; Jayasree, E. G. *Acc. Chem. Res.* **2003**, *36*, 816.